scientific reports

OPEN

Influence of InP coupling cavity on Fano resonance of sub wavelength MIM waveguide

Shihao Ban[1], Huangqing Liu[1✉], Shifang Xiao[1], Jingjing Mao[2✉] & Jie Luo[3]

In this paper, influence of InP coupling cavity on Fano resonance of sub wavelength MIM waveguide was studied by FDTD. It was observed that the resonant wavelengths of mode m_j (j = 1, 2, 3) were closely related with the height H_2 of InP coupling cavity. In addition, before and after the addition of air cavity, the relative farfield intensities I was a function of height H_2. Therefore, InP as discrete state could be used as the filling dielectrics of Fano resonance in the MIM waveguide.

Due to its attractive features and extensive applications, the metal–insulator–metal (MIM) waveguide[1–5] were very popular with researchers. During the process of light propagation in the nano-photonic circuits, MIM waveguides could reduce energy loss. The MIM waveguide with coupling cavity could change its filtering performance[6–9], such as Fano resonance. The most common structures with the filters were MIM waveguides with a rectangular cavity[10–14]. Silicon was used as filter dielectrics in the coupling cavity[13,14]. Due to relatively large dielectric constant and high-order resonance about 1700 nm in the near-infrared region, silicon was usually regarded as discrete state of Fano resonance[13–18]. In the study, obvious Fano resonance could be observed when InP was chose as the dielectrics in the coupling cavity of MIM waveguide. Namely, InP could also be used as discrete state of Fano resonance. In this paper, InP[19–25] would be used as the filling dielectrics in the MIM waveguide cavity and the influence of InP coupling cavity on Fano resonance of sub wavelength MIM waveguide (Ag-Air-Ag) was explored on the basis of the literatures[22,25,26].

Results

The sketch of the waveguide structure designed was shown in Fig. 1. In the figure, the distance w of the main waveguide cavity with the transparent dielectrics (n = 1.0) was set as 50 nm which was far less than the wavelength λ of incident wave so that SPPs propagation mode could be excited in MIM waveguide structure because the number of SPP modes was closely related to the distance along the wave propagation direction[27]. In addition, the width L of the coupled cavities was also set as 50 nm. Our simulation results indicated that Fano resonance was independent of the horizontal distance between the two cavities and dependent on the height H_1 (H_2). Additionally, the relative far-field intensity I was defined as the area under the far-field curve and was proportional to the height h of the curve in this paper.

Figure 2a showed the transmission spectra under different InP structures without air cavity **A**. It could be observed that the resonance peaks of mode m_j (j = 1, 2, 3) redshifted with the increase of H_2 from 240 to 350 nm. And that the resonant wavelengths were a function of the height H_2. Take H_2 = 350 nm as an example, it could be observed three resonance valleys at about 998 nm, 1302 nm and 2079 nm, respectively. The resonance valleys at 1302 nm and 2079 nm were considered to be first and second order resonance modes, shown in Fig. 2c,d. However, the resonance valley at 998 nm was regarded as third-order resonance (seen in Fig. 2a,b), which was independent of the height H_1 and closely related to the height H_2 according to our simulations. In other words, the resonance mode in Fig. 2a could directly be confirmed by the distribution of magnetic field in Fig. 2b–d.

When the zero order dark mode from the Air cavity and j-order bright modes (j = 1, 2 and 3) from the InP cavity were superimposed, some Fano resonance of the modes m_j (j = 1, 2 and 3) could be obtained in Fig. 3a, which showed the transmission spectra of different InP-Air structures. In the case of only air cavity, the transmission spectrum was very wide passband, which covered the resonance wavelengths of the modes m_j (j = 1, 2 and 3) and whose central wavelength was lied at about 1710 nm. For the mode m_1, more obvious Fano resonance was observed when H_2 = 240 nm and 260 nm. However, the most obvious Fano resonance came from the mode m_2 whose resonance valley shifted to the long wavelength with the H_2 increase. According to the main

[1]School of Physics and Electronics, Hunan University, Changsha 410082, People's Republic of China. [2]Huaihua Normal College, Huaihua 418008, People's Republic of China. [3]School of Material Science and Engineering, Central South University of Forestry and Technology, Changsha 410004, Hunan, People's Republic of China. ✉email: lhq468@sohu.com; mjj6937213@163.com
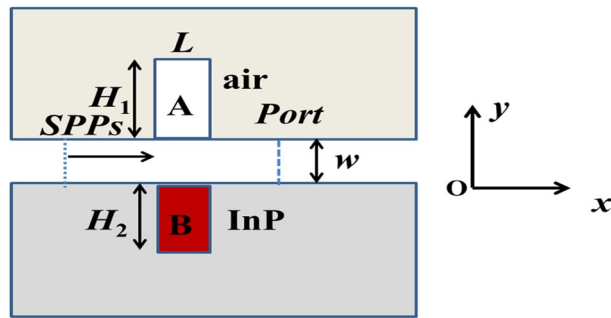
Figure 1. Research scheme and design schematic of 2D simulation. The capital letters A and B denote air and InP coupled cavities, respectively. The structural parameters were $L = w = 50$ nm.
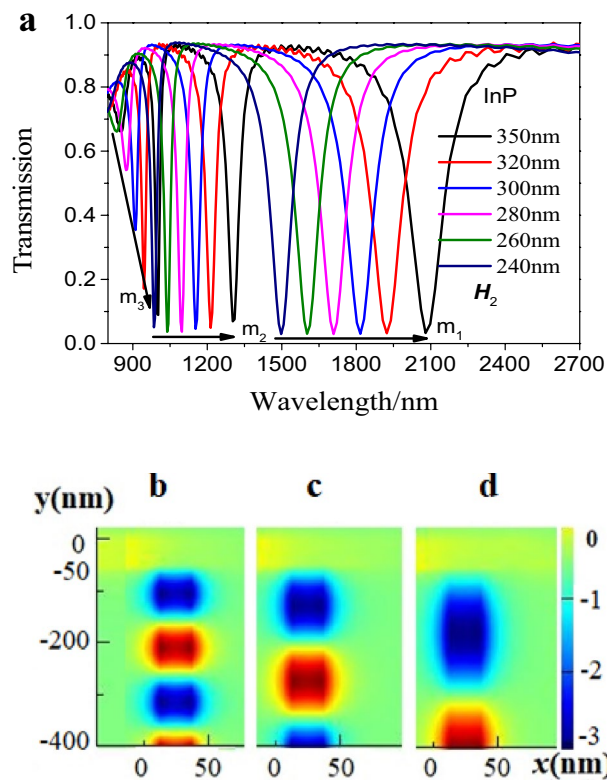

Figure 2. (**a**) The relation between Fano resonance and the height H_2. (**b–d**) Magnetic field distribution of different modes at different resonance wavelengths 998 nm, 1302 nm and 2079 nm, respectively. Red and blue represent two different vibrations. The structural parameter was $H_2 = 350$ nm.

resonance peak[22–23] of the mode m_2 in the Fig. 3a, the quality factor (QF) and the extinction ratio (ER) could be calculated[19,20,23,26]. The quality factor Q was defined as the ratio of the resonance wavelength λ_0 and the full width $\Delta\lambda$ between the peak and the antipeak of the transmission ($Q = \lambda_0/\Delta\lambda$). The extinction ratio (Ext) was ten times the logarithm of the ratio of the maximum transmission light intensity P to the minimum transmitted light intensity P_0, namely, Ext $= 10\lg(P/P_0)$. A high-quality factor meant lower light energy loss in a resonant cavity. Moreover, the lager extinction ratio was implied the better quality of the resonator. For the different InP-Air structures with the length H_2 from 240 to 350 nm (240 nm, 260 nm, 280 nm, 300 nm, 320 nm and 350 nm), the quality factor QFs calculated were about 44, 30, 29, 28, 34 and 37, respectively. The ERs obtained were around 13, 18, 15, 14, 31 and 12 dB, respectively. These results showed that the QFs and the ERs were a function of the height H_2. There was lower light energy loss in a resonant cavity and better quality of the resonator for the length $H_2 = 240$ nm and 320 nm. In other words, when the height H_2 was not higher than 240 nm and not less than 320 nm, the waveguide structure with InP-Air cavities had good filtering performance. In addition, it was obtained that the addition of air cavity did not change the resonant position which was dependent on structure sizes of the cavity InP. Take $H_2 = 350$ nm as an example, for the three resonance valleys at 998 nm, 1302 nm and 2079 nm, it was observed the magnetic field distribution did not change before and after the addition of air
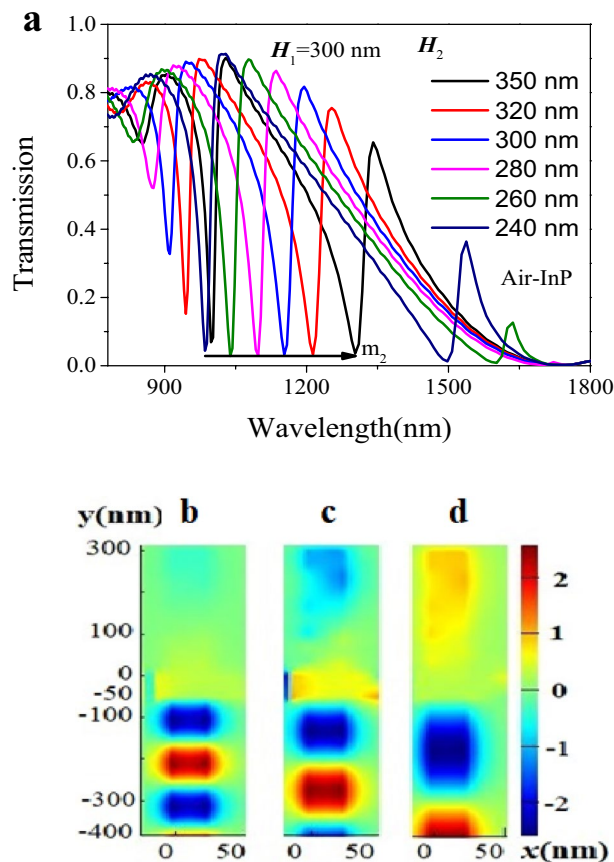
Figure 3. (**a**) The relationship between Fano resonance and the height H_2 in the range from 780 to 1800 nm. (**b**–**d**) Magnetic field distribution of different modes at different resonance wavelengths 998 nm, 1302 nm and 2079 nm, respectively. Red and blue represent two different vibrations. The structural parameter was $H_1 = 300$ nm.

cavity. Additionally, it was obtained that the magnetic field distribution of the zero-order resonance in the air cavity, as shown in Fig. 3b–d.

Before the addition of air cavity, under 1302.87 nm monitoring, the relative farfield intensities I varied with the height H_2 from 240 to 350 nm and was a function of height H_2, namely, $I = I(H_2)$, as shown in Fig. 4a. The shape of the curve was Guassian Spot with periodic structure, whose symmetric center was located at about $\theta = -2.2°$, as shown in the black dash. The relative farfield intensity I gradually decreased with the height H_2 from 260 to 350 nm. The maximum relative intensity $I(260)$ was about three times that of the minimum $I(350)$, $I(260) = 3I(350)$. After the addition of air cavity, it was observed that the relative farfield intensities I was also a function of height H_2, as shown in Fig. 4b. The symmetric center of the curve with periodic structure was located at about $\theta = 0°$, as seen in the black dash. The relative farfield intensity I gradually increased with the height H_2 from 240 to 320 nm. The maximum relative intensity $I(320)$ was about four times that of the minimum $I(350)$, namely, $I(320) = 4I(350)$. Therefore, the change of structural parameters could be obtained according to the change of far-field relative intensity[20].

Discussion

Influence of InP coupling cavity on Fano resonance of sub wavelength MIM waveguide was studied in this paper. Some novel results were obtained. For different InP structures without air cavity, it was observed the resonance peaks of mode m_j (j = 1, 2 and 3) redshifted with H_2 increase and the resonant wavelengths of mode m_j (j = 1, 2 and 3) were a function of the height H_2. For the different InP-Air structures with the length H_2 from 240 to 350 nm, the resonance valley of the mode m_2 shifted to the long wavelength. In addition, before and after the addition of air cavity, the relative farfield intensities I was a function of the height H_2. Therefore, InP as discrete state of Fano resonance could be used as the filling dielectrics of Fano resonance in the MIM waveguide.

Methods

Numerical simulations. In the letter, the MIM plasmonic waveguide coupled with InP cavity was investigated using the finite-difference time-domain (FDTD, Lumerical Computational Solutions Incorporation) with a perfectly matched layer absorbing boundary condition. A plane wave with the electric field parallel to the x axis illuminates normally the periodic structure. The grid sizes in the x and y directions were 2 nm.
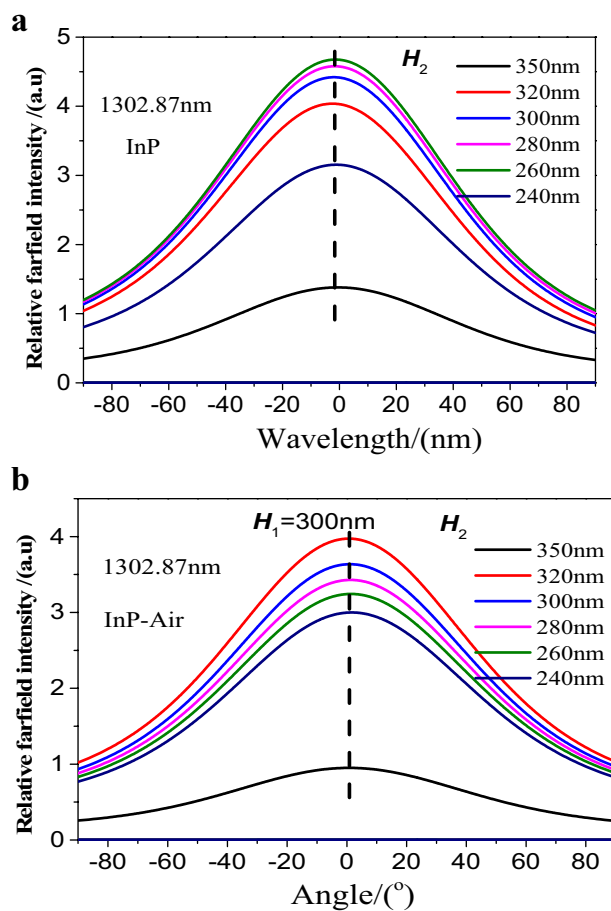
Figure 4. Farfield with vavious angle from − 90° to 90° and changeable height H_2 from 240 to 350 nm before (**a**) and after (**b**) the addition of air cavity under 1302.87 nm monitoring.

References

1. Törmä, P. & Barnes, W. L. Strong coupling between surface plasmon polaritons and emitters: A review. *Rep. Prog. Phys.* **78**, 013901. https://doi.org/10.1088/0034-4885/78/1/013901 (2015).
2. Abdol, S. O. *et al.* Tunable surface plasmon polaritons in a Weyl semimetal waveguide. *J. Phys. Condens. Matter* **31**, 335002. https://doi.org/10.1088/1361-648X/ab217f (2019).
3. Lošić, ŽB. Surface plasmons in Weyl semimetals. *J. Phys. Condens. Matter* **30**, 365003. https://doi.org/10.1088/1361-648X/aad6f5 (2018).
4. Saleh, N. M. & Aziz, A. A. Simulation of surface plasmon resonance on different size of a single gold nanoparticle. *J. Phys. Conf. Ser.* **1083**, 012041. https://doi.org/10.1088/1742-6596/1083/1/012041 (2018).
5. Cao, E. *et al.* Exciton–plasmon hybrids for surface catalysis detected by SERS. *Nanotechnology* **29**, 372001. https://doi.org/10.1088/1361-6528/aacec4 (2018).
6. Melentev, G. A. *et al.* Surface plasmon-phonon polaritons in GaAs. *J. Phys. Conf. Ser.* **917**, 062038. https://doi.org/10.1088/1742-6596/917/6/062038 (2017).
7. Kim, Y. *et al.* Demonstration of integrated polarization rotator based on an asymmetric silicon waveguide with a trench. *J. Opt.* **18**, 095801. https://doi.org/10.1088/2040-8978/18/9/095801 (2016).
8. Ghosh, S. *et al.* Transverse localization of light in 1D disordered waveguide lattices in the presence of a photonic bandgap. *Laser Phys.* **24**, 045001. https://doi.org/10.1088/1054-660X/24/4/045001 (2014).
9. Piccione, B. *et al.* Tailoring light–matter coupling in semiconductor and hybrid-plasmonic nanowires. *Rep. Prog. Phys.* **77**, 086401. https://doi.org/10.1088/0034-4885/77/8/086401 (2014).
10. Wen, K. *et al.* Wavelength demultiplexing structure based on a plasmonic metal–insulator–metal waveguide. *J. Opt.* **14**, 075001. https://doi.org/10.1088/2040-8978/14/7/075001 (2012).
11. Sheng, Y. *et al.* Fabrication of lateral electrodes on semiconductor nanowires through structurally matched insulation for functional optoelectronics. *Nanotechnology* **24**, 025204. https://doi.org/10.1088/0957-4484/24/2/025204 (2013).
12. Yun, B., Hu, G. & Wei, C. J. Plasmon induced transparency in metal–insulator–metal waveguide by a stub coupled with F-P resonator. *Mater. Res. Express* **1**, 036201. https://doi.org/10.1088/2053-1591/1/3/036201 (2014).
13. Zhong, X. & Li, Z. Plasmon enhanced light amplification in metal–insulator–metal waveguides with gain. *J. Opt.* **14**, 055002. https://doi.org/10.1088/2040-8978/14/5/055002 (2012).
14. Wang, Y. & Yan, X. Mode conversion in metal–insulator–metal waveguide with a shifted cavity. *Jpn. J. Appl. Phys.* **57**, 010303 (2018).
15. Zheng, G., Su, W. & Chen, Y. Band-stop filters based on a coupled circular ring metal–insulator–metal resonator containing nonlinear material. *J. Opt.* **14**, 055001. https://doi.org/10.1088/2040-8978/14/5/055001 (2012).

16. Nurmohammadi, T. *et al.* Ultra-fast all-optical plasmon induced transparency in a metal–insulator–metal waveguide containing two Kerr nonlinear ring resonators. *J. Opt.* **20**, 055504. https://doi.org/10.1088/2040-8986/aab882 (2018).
17. Yun, B., Hu, G. & Cui, Y. Theoretical analysis of a nanoscale plasmonic filter based on a rectangular metal–insulator–metal waveguide. *J. Phys. D Appl. Phys.* **43**, 385102 (2010).
18. Li, S., Liu, H. & Liu, L. Effect of silver film thickness on the surface plasma resonance in the rectangular Ag–Si–SiO$_2$ cavity. *J. Phys. Commun.* **2**, 055024. https://doi.org/10.1088/2399-6528/aac52e (2018).
19. Li, S. *et al.* Investigation of surface plasmon resonance in the rectangular cavity of Ag–Si–SiO$_2$. *Plasmonics* **13**(6), 2313. https://doi.org/10.1007/s11468-018-0754-y (2018).
20. Li, S. *et al.* Farfield under small scattering angle in the rectangular Ag–Si–SiO$_2$ cavity. *Plasmonics* **14**, 1385. https://doi.org/10.1007/s11468-019-00928-7 (2019).
21. Ghorbani, S., Dashti, M. A. & Jabbar, M. Plasmonic nano-sensor based on metal-dielectric-metal waveguide with the octagonal cavity ring. *Laser Phys.* **28**, 066208. https://doi.org/10.1088/1555-6611/aab463 (2018).
22. Mao, J. *et al.* Numerical analysis of near-infrared plasmonic filter with high figure of merit based on Fano resonance. *Appl. Phys. Express* **10**, 082201. https://doi.org/10.7567/APEX.10.082201 (2017).
23. Zhang, S., Li, G. & Chen, Y. Pronounced fano resonance in single gold split nanodisks with 15 nm split gaps for intensive second harmonic generation. *ACS Nano* **10**, 11105–11114. https://doi.org/10.1021/acsnano.6b05979 (2016).
24. Ren, D. K., Farrell, C. A., Diana, L. & Huffaker, L. Axial InAs(Sb) inserts in selective-area InAsP nanowires on InP for optoelectronics beyond 2.5 µm. *Opt. Mater. Express* **8**(4), 1075–1081. https://doi.org/10.1364/OME.8.001075 (2018).
25. Bekele, D. A. *et al.* Optical time domain demultiplexing using fano resonance in InP photonic crystals. In *The European Conference on Lasers and Electro-Optics, Paper* CK_1_5 (2017).
26. Li, S. *et al.* Fano resonance of air-Si waveguide cavity. *Plasma Res. Express* **2**(4), 045005. https://doi.org/10.1088/2516-1067/abc467 (2020).
27. Li, H. *et al.* Graphene-based mid-infrared, tunable, electrically controlled plasmonic filter. *Appl. Phys. Express* **7**, 024301. https://doi.org/10.7567/APEX.7.024301 (2014).

Acknowledgements

Author contributions

J.J.M. designed the Fig. 1. S.H.B. made a simulation according to the design and processed the pictures of the simulated magnetic field (Figs. 2b–d, 3b–d) by using drawing software. H.Q.L made the figures (Figs. 2a, 3a, 4a,b) by using OriginPro 9.0 according to the simulated data and participated in the analysis and interpretation of all figures. All the authors participated in the writing of the article. S.F.X. and J.L. provided financial support.

Competing interests

The authors declare no competing interests.

Additional information

Correspondence and requests for materials should be addressed to H.L. or J.M.

Reprints and permissions information is available at www.nature.com/reprints.

Publisher's note Springer Nature remains neutral with regard to jurisdictional claims in published maps and institutional affiliations.